International Journal of Thermal Sciences 48 (2009) 1755–1764

Contents lists available at ScienceDirect

International Journal of Thermal Sciences

journal homepage: www.elsevier.com/locate/ijts

Mathematical modelling of a LiBr–H_2O absorption chiller including two-dimensional distributions of temperature and concentration fields for heat and mass exchangers

Krzysztof Banasiak*, Joachim Kozioł

Institute of Thermal Technology, Silesian University of Technology, Konarskiego 22, Gliwice 44-100, Poland

ARTICLE INFO

Article history:
Received 25 June 2008
Received in revised form
18 November 2008
Accepted 23 January 2009
Available online 14 March 2009

Keywords:
Absorption chiller
Crosscurrent flow
LiBr–H_2O solution
Mass diffusion

ABSTRACT

The paper presents the results of a theoretical analysis performed for a single-stage, water–lithium bromide absorption chiller at steady-state conditions. The model takes into consideration crosscurrent flow of fluids for heat and mass exchangers, two-dimensional distribution of temperature and concentration fields, local values of heat and mass transfer coefficients, thermal-parameter-dependent physical properties of working fluids and operation limits due to the danger of the LiBr–water hydrates and ice crystallisation. The main practical advantage of the model is the possibility to assess the influence of both the geometry parameters and operation parameters on thermal performance of the absorption chiller. The results derived from the implementation of the water vapour absorption process model for a horizontal tube absorber are consistent with the experimental measurements found in the literature.

© 2009 Elsevier Masson SAS. All rights reserved.

1. Introduction

In the vast majority of the mathematical models of the water–lithium bromide absorption chillers the simulation procedures are based only on the mass and energy balances, equations of state and equations of heat transfer, e.g. in refs. [6,10], which implies the governing equations for the processes of mass transfer by diffusion are neglected. In fact, the number of reported researches including mathematical modelling of diffusion processes is fairly limited [7,9]. Moreover, the heat transfer formulae are commonly used in a simplified, dimensionless form of the heat transfer effectiveness or the logarithmic mean temperature difference [1,11,20]. However, in practice, heat transfer should be analysed as a three-dimensional problem, mainly due to the non-uniform distribution of a temperature difference between the working fluids. Therefore, unlike in the case of zero-dimensional algebraic equations of state or balance equations, the heat (and desirably mass) transfer equations should be considered partial differential equations due to the vectorial character of heat and mass flux. On the other hand, such a method would impose the necessity of integration of differential equations at strictly specified boundary conditions in every performed simulation, which would lengthen the computation time significantly. Another difficulty is an enormous disproportion in geometrical scale between the volume of a typical sorption exchanger and the characteristic dimension of heat and mass transfer zones. Large area of heat/mass transfer and ultra low thickness of heat/mass transfer layers causes the three-dimensional modelling is extremely complicated. This fact actually limits practical importance of the absorption unit models based on a full three-dimensional heat and mass transfer analysis for a complete heat and mass exchanger, e.g. an absorber, mainly when bearing in mind robustness and simplicity of the zero-dimensional models.

Nevertheless, several attempts have been made to create a model that would join the computational effectiveness of procedures with the non-uniform distribution of driving forces for heat and mass transfer on the sorption exchangers. This resulted in procedures for calculations of one-dimensional [7] or pseudo two-dimensional [9] fields of thermal parameters for the heat and mass exchange surface area. Hellmann and Grossman in ref. [7] carried out a series of numerical simulations for a model of the open cycle air–water dehumidifier–evaporator–regenerator absorption refrigerator. In this work the dehumidifier operating as an absorber and regenerator working as a desorber were modelled as one-dimensional counter-current heat and mass exchangers. Joudi and Lafta in ref. [9] developed a model of a LiBr–H_2O absorption chiller where the absorption process was modelled as the pseudo cross-current heat and mass transfer on a horizontal tube bank. The heat and mass transfer phenomena for gravitational solution flow

* Corresponding author. Tel.: +48 32 237 1019; fax: +48 32 237 2872.
E-mail address: krzysztof.banasiak@polsl.pl (K. Banasiak).

1290-0729/$ – see front matter © 2009 Elsevier Masson SAS. All rights reserved.
doi:10.1016/j.ijthermalsci.2009.01.018

Nomenclature

A	active surface area of mass/heat transfer, m^2
C_1, C_2	coefficients in Eq. (26), explained in Eqs. (27) and (28)
c	specific heat capacity, J kg^{-1} K^{-1}
$\dot{G}$	mass flow rate, kg s^{-1}
g	gravitational acceleration, $g = 9.81$ m s^{-2}
h	specific enthalpy, J kg^{-1}
U_l	overall heat transfer coefficient in cylindrical coordinates, W m^{-1} K^{-1}
L	total tube length, m
l	linear coordinate (along tube length), m
N	power of the solution pump, W
p	pressure, Pa
$\dot{Q}$	heat transfer rate, W
t	temperature, °C
W	ratio of the mass of water to the mass of pure lithium bromide
X	mass fraction
δ	laminar film thickness, m
ζ	dimensionless linear coordinate, $\zeta = l/L$
η	efficiency of solution pump
ν	kinematic viscosity, m^2 s^{-1}
Θ	total angle of a gravitational flow along the tube perimeter, rad
θ	angular coordinate (angle between the vertical and a normal to the tube surface), rad
π	Ludolphian number, $\pi = 3.141593\ldots$
ρ	density, kg m^{-3}
χ_1	overall mass transfer coefficient in cylindrical coordinates (expressed with respect to ΔW), kg m^{-1} s^{-1}
ψ	dimensionless angular coordinate, $\psi = \theta/\pi$
Re	Reynolds number
Sc	Schmidt number
Sh	Sherwood number

Subscripts

ABS	absorber
CND	condenser
cw	cooling water
DES	desorber
dif	transported by diffusion
el	electric
em	electromechanical
eq	equilibrium state
es	external surface
EVP	evaporator
LiBr	pure lithium bromide
s	isentropic
SHX	solution heat exchanger
sol	solution
v	water vapour
w	liquid water

Superscripts

$'$	saturated liquid
$''$	saturated vapour

crossways a horizontal tube were simplified to the analysis for a flow along a vertical isothermal plate, while the mechanism of the mass diffusion was modelled with the mass transfer coefficients determined from the dimensionless analogy mass transfer numbers.

Hence, the main purpose of the present paper is to go beyond the existing limitations in absorption chillers operation modelling and to enhance the previous models with aspects of the field analysis. Therefore, a general objective of the paper is to develop a steady-state mathematical model of the industrial sorption refrigeration system including two-dimensional distributions of temperature and concentration fields for heat and mass exchangers.

The main computational improvement the authors introduce is a numerical approach. The time-consuming continual procedures of numerical integration of differential equations for every operation point were substituted by means of a single series calculations performed for the most representative set of the input data (i.e. operation parameters like the inlet mass flow rates, inlet temperature, inlet pressure, inlet concentration). Subsequently, the obtained results were approximated for each heat/mass exchanger by means of multivariable second-order polynomials (a detailed description of the approximating functions derivation is given in Section 3), valid for a given geometry. Thus, bearing in mind possible discrepancies among the results of detailed integration and approximation as well as the necessity of repeating the whole scheme for a different geometry, it is possible to replace differential equations with algebraic equations, far more convenient for a procedure of solution of a non-linear set of equations.

The results of numerical simulations presented in the paper include both detailed distributions of thermal-parameters on heat and mass exchangers as well as general characteristics of energy performance as the refrigeration capacity and coefficient of performance. Multivariable operating characteristics may be especially valuable for the pre-investment feasibility analyses including energy and financial estimations performed for both rated and part-load exploitation conditions.

2. Mathematical modelling of the water–lithium bromide sorption cycles

The procedure of mathematical modelling was performed at two distinct levels of the analysis: the external level of zero-dimensional energy and mass balancing and internal level of two-dimensional heat/mass transfer fluxes determination for each heat/mass exchanger (see Fig. 1). The external level was continually computed at each simulated operating point, while the internal level was pre-executed only once for a given chiller geometry. Based on the results of the internal level simulations, the approximation functions for heat and mass transfer were incorporated into the zero-dimensional model. For this reason the computation procedure could be limited strictly to the solution of the algebraic non-linear equations system.

The zero-dimensional model of the LiBr–H_2O absorption chiller was derived from the energy analysis of a typical industrial single-stage unit (Fig. 2), which consists of the refrigeration part (II–III–IV–V) and the thermal pump part (VI–VII–VIII–IX–I). A typical stream configuration embraces the pure refrigerant stream (points 9–10–11–12), strong solution stream (points 5–6), weak solution stream (points 1–2–3–4), intermediate solution stream (points 7–8), chilling water stream (points 13–14), cooling water stream (points 15–16–17) and driving hot water stream (points 18–19).

The fundamental simplifications assumed for the analysis were as follows [6,9–11]:

- steady-state operation;
- water as a pure refrigerant;

○ no heat losses through the device jacket;
○ total enthalpy composed of thermal energy only (kinetic and potential energy components are neglected);
○ no radiation heat transfer;
○ no pressure losses except the flow restrictor (III), evaporator nozzles and absorber nozzles;
○ isenthalpic pressure reduction in the flow restrictor (III);
○ saturated vapour flowing from the evaporator (IV) into the absorber (VII);
○ solution jet pump (VI) modelled as a simple flow mixer.

The input data set includes the following construction and geometry information as well as operation parameters (see Fig. 2):

○ number, construction material, spatial arrangement (pitch), surface structure, internal and external diameter as well as length of the tubes in each of four basic exchangers: absorber (VII), desorber (I), evaporator (IV) and condenser (II);
○ operation characteristic of a mechanical solution pump (VIII);
○ mass flow rate ($\dot{G}_{18} = \dot{G}_{19}$), temperature ($t_{18}$) and pressure ($p_{18} = p_{19}$) values of hot water at inlet;
○ mass flow rate ($\dot{G}_{15} = \dot{G}_{16} = \dot{G}_{17}$), temperature ($t_{15}$) and pressure ($p_{15} = p_{16} = p_{17}$) values of cooling water at inlet;
○ mass flow rate ($\dot{G}_{13} = \dot{G}_{14}$), temperature ($t_{13}$) and pressure ($p_{13} = p_{14}$) values of chilling water at inlet;
○ electric power of the mechanical solution pump (N_{el}) or circulation ratio $\left(\frac{\dot{G}_4}{\dot{G}_9}\right)$.

As a result, the total number of unknowns in the model reached 21, namely:

○ pressure of absorption ($p_1 = p_8 = p_{11} = p_{12}$) and pressure of desorption ($p_2 = p_3 = p_4 = p_5 = p_6 = p_7 = p_9 = p_{10}$);
○ mass flow rate ($\dot{G}_7 = \dot{G}_8$), temperature ($t_7 = t_8$) and LiBr concentration ($X_{\text{LiBr }7} = X_{\text{LiBr }8}$) values for the absorber inlet;
○ mass flow rate ($\dot{G}_1 = \dot{G}_2$), temperature ($t_1 = t_2 = t_3$) and LiBr concentration ($X_{\text{LiBr }1} = X_{\text{LiBr }2} = X_{\text{LiBr }3} = X_{\text{LiBr }4}$) values for the absorber outlet;
○ mass flow rate ($\dot{G}_5 = \dot{G}_6$), temperature (t_5) and LiBr concentration ($X_{\text{LiBr }5} = X_{\text{LiBr }6}$) values for the desorber outlet as well as mass flow rate ($\dot{G}_4$) and temperature (t_4) values for the desorber inlet;
○ mass flow rate of weak solution flowing into the jet pump ($\dot{G}_3$);
○ temperature of strong solution flowing out of the solution heat exchanger (t_6);
○ temperature of water vapour flowing into the condenser (t_9);
○ temperature of cooling water flowing out of the absorber (t_{16});

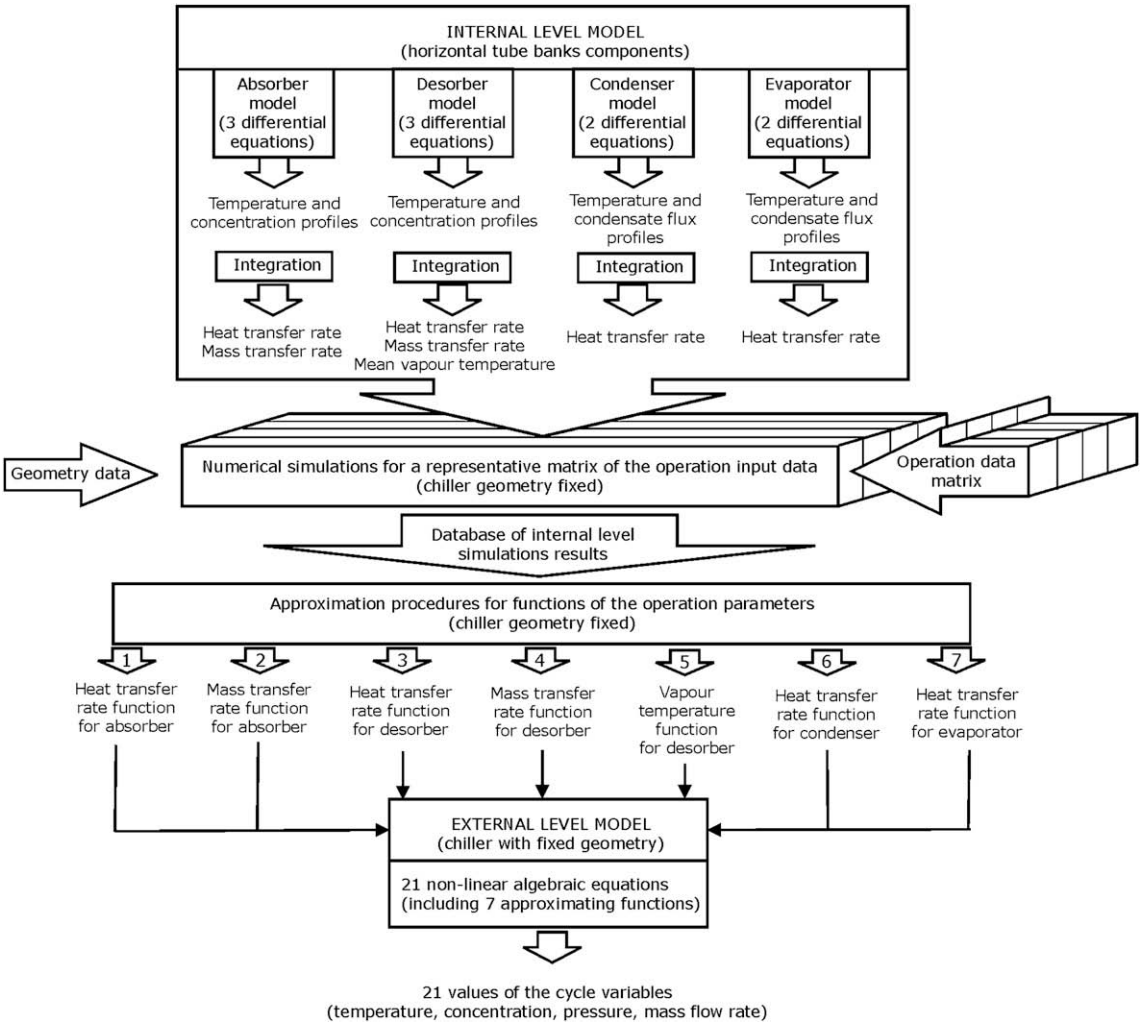

Fig. 1. Schematic representation of the two-level model structure.

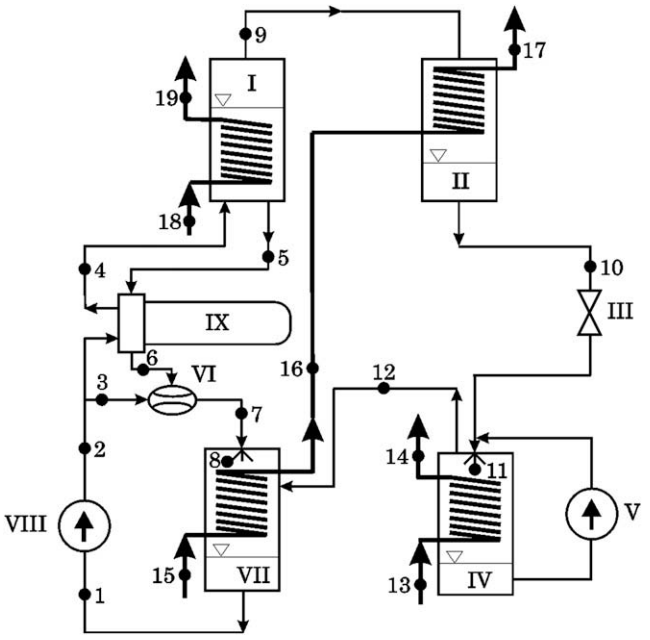

Fig. 2. Schematic representation of a single-stage LiBr–H_2O absorption chiller (for the sake of the scheme simplicity all horizontal tube banks were replaced with the representation of coil pipes); I – steam generator (desorber), II – condenser, III – flow restrictor (throttle valve), IV – falling-film evaporator, V – condensate pump, VI – solution jet pump (strong/weak solution flows mixer), VII – falling-film absorber, VIII – solution mechanical pump, IX – strong/weak solution heat exchanger; values expressed by Arabic numerals refer to the characteristic points of the cycle.

- temperature of cooling water flowing out of the condenser (t_{17});
- temperature of hot water flowing out of the desorber (t_{19});
- temperature of chilling water flowing out of the evaporator (t_{14});
- mass flow rate of refrigerant ($\dot{G}_9 = \dot{G}_{10} = \dot{G}_{11} = \dot{G}_{12}$).

To solve the problem the non-linear model was based on the following 21 algebraic equations:

■ the overall mass balance (Eq. (1)) and LiBr mass balance (Eq. (2)) for the absorber;

$$\dot{G}_7 + \dot{G}_9 = \dot{G}_1 \tag{1}$$

$$\dot{G}_7 X_{\mathrm{LiBr}\,7} = \dot{G}_1 X_{\mathrm{LiBr}\,1} \tag{2}$$

■ the overall mass balance (Eq. (3)) and LiBr mass balance (Eq. (4)) for the desorber;

$$\dot{G}_4 = \dot{G}_5 + \dot{G}_9 \tag{3}$$

$$\dot{G}_4 X_{\mathrm{LiBr}\,1} = \dot{G}_5 X_{\mathrm{LiBr}\,5} \tag{4}$$

■ the overall mass balance (Eq. (5)) and LiBr mass balance (Eq. (6)) for the jet pump;

$$\dot{G}_3 + \dot{G}_6 = \dot{G}_7 \tag{5}$$

$$\dot{G}_3 X_{\mathrm{LiBr}\,1} + \dot{G}_6 X_{\mathrm{LiBr}\,5} = \dot{G}_7 X_{\mathrm{LiBr}\,7} \tag{6}$$

■ energy balances for the absorber (Eq. (7)), desorber (Eq. (8)), condenser (Eq. (9)), evaporator (Eq. (10)), jet pump (Eq. (11)) and solution heat exchanger (Eq. (12));

$$\dot{G}_7 h_{\mathrm{sol}}(t_7, X_{\mathrm{LiBr}\,7}) + \dot{G}_9 h''_{\mathrm{v}}(p_1) + \dot{G}_{15} h_{\mathrm{w}}(p_{15}, t_{15}) = \dot{G}_1 h_{\mathrm{sol}}(t_1, X_{\mathrm{LiBr}\,1}) + \dot{G}_{15} h_{\mathrm{w}}(p_{15}, t_{16}) \tag{7}$$

$$\dot{G}_4 h_{\mathrm{sol}}(t_4, X_{\mathrm{LiBr}\,1}) + \dot{G}_{18} h_{\mathrm{w}}(p_{18}, t_{18}) = \dot{G}_5 h_{\mathrm{sol}}(t_5, X_{\mathrm{LiBr}\,5}) + \dot{G}_{18} h_{\mathrm{w}}(p_{18}, t_{19}) + \dot{G}_9 h_{\mathrm{v}}(p_2, t_9) \tag{8}$$

$$\dot{G}_9 h_{\mathrm{v}}(p_2, t_9) + \dot{G}_{15} h_{\mathrm{w}}(p_{15}, t_{16}) = \dot{G}_9 h'_{\mathrm{w}}(p_2) + \dot{G}_{15} h_{\mathrm{w}}(p_{15}, t_{17}) \tag{9}$$

$$\dot{G}_9 h'_{\mathrm{w}}(p_2) + \dot{G}_{13} h_{\mathrm{w}}(p_{13}, t_{13}) = \dot{G}_9 h'_{\mathrm{v}}(p_1) + \dot{G}_{13} h_{\mathrm{w}}(p_{13}, t_{14}) \tag{10}$$

$$\dot{G}_3 h_{\mathrm{sol}}(t_1, X_{\mathrm{LiBr}\,1}) + \dot{G}_5 h_{\mathrm{sol}}(t_6, X_{\mathrm{LiBr}\,5}) = \dot{G}_7 h_{\mathrm{sol}}(t_7, X_{\mathrm{LiBr}\,7}) \tag{11}$$

$$\dot{G}_4 h_{\mathrm{sol}}(t_1, X_{\mathrm{LiBr}\,1}) + \dot{G}_5 h_{\mathrm{sol}}(t_5, X_{\mathrm{LiBr}\,5}) = \dot{G}_4 h_{\mathrm{sol}}(t_4, X_{\mathrm{LiBr}\,1}) + \dot{G}_5 h_{\mathrm{sol}}(t_6, X_{\mathrm{LiBr}\,5}) \tag{12}$$

■ hydraulic energy balance of the solution pump (Eq. (13)), including internal and electromechanical efficiency;

$$N_{\mathrm{el}} = \frac{\dot{G}_1}{\eta_{\mathrm{s}} \eta_{\mathrm{em}} \rho_{\mathrm{sol}}(t_1, X_1)} (p_2 - p_1) \tag{13}$$

■ heat and mass transfer rates for the absorber (Eqs. (14) and (15)) and desorber (Eqs. (16) and (17)) – multivariable second-order polynomials derived by means of an approximation procedure from the numerically integrated differential heat and mass transfer equations (detailed description of the approximating functions derivation is given in Section 3),

$$\int_{A_{\mathrm{ABS}}} \mathrm{d}\dot{Q} = \dot{Q}_{\mathrm{ABS}}(p_1, \dot{G}_7, t_7, X_{\mathrm{LiBr}\,7}, \dot{G}_{15}, t_{15}) = \dot{G}_{15} h_{\mathrm{w}}(p_{15}, t_{16}) - \dot{G}_{15} h_{\mathrm{w}}(p_{15}, t_{15}) \tag{14}$$

$$\int_{A_{\mathrm{ABS}}} \mathrm{d}\dot{G}_{\mathrm{dif}} = \dot{G}_{\mathrm{dif\ ABS}}(p_1, \dot{G}_7, t_7, X_{\mathrm{LiBr}\,7}, \dot{G}_{15}, t_{15}) = \dot{G}_9 \tag{15}$$

$$\int_{A_{\mathrm{DES}}} \mathrm{d}\dot{Q} = \dot{Q}_{\mathrm{DES}}(p_2, \dot{G}_4, t_4, X_{\mathrm{LiBr}\,1}, \dot{G}_{18}, t_{18}) = \dot{G}_{18} h_{\mathrm{w}}(p_{18}, t_{18}) - \dot{G}_{18} h_{\mathrm{w}}(p_{18}, t_{19}) \tag{16}$$

$$\int_{A_{\mathrm{DES}}} \mathrm{d}\dot{G}_{\mathrm{dif}} = \dot{G}_{\mathrm{dif\ DES}}(p_2, \dot{G}_4, t_4, X_{\mathrm{LiBr}\,1}, \dot{G}_{18}, t_{18}) = \dot{G}_9 \tag{17}$$

■ mean temperature of vapour generated inside the desorber (Eq. (18)) – multivariable second-order polynomial derived using an approximation procedure from the mean value of an area integral;

$$\frac{\int_{A_{\mathrm{DES}}} t_{\mathrm{v}}\, \mathrm{d}A}{A_{\mathrm{DES}}} = t_{\mathrm{v\ DES}}(p_2, \dot{G}_4, t_4, X_{\mathrm{LiBr}\,1}, \dot{G}_{18}, t_{18}) = t_9 \tag{18}$$

■ heat transfer rates for the condenser (Eq. (19)) and evaporator (Eq. (20)) – multivariable second-order polynomials derived by

means of approximation procedure from the numerically integrated differential heat transfer equations;

$$\int_{A_{CND}} d\dot{Q} = \dot{Q}_{CND}(p_2,\ t_9,\ \dot{G}_{15},\ t_{16}) = \dot{G}_{15}h_w(p_{15},\ t_{17}) - \dot{G}_{15}h_w(p_{15},\ t_{16}) \quad (19)$$

$$\int_{A_{EVP}} d\dot{Q} = \dot{Q}_{EVP}(p_1,\ \dot{G}_{13},\ t_{13}) = \dot{G}_{13}h_w(p_{13},\ t_{13}) - \dot{G}_{13}h_w(p_{13},\ t_{14}) \quad (20)$$

■ heat transfer rate for the solution heat exchanger (Eq. (21)) – analytical solution for the counter-current heat exchanger.

$$\dot{Q}_{SHX}(\dot{G}_4,\ t_1,\ X_{LiBr\ 1},\ \dot{G}_5,\ t_5,\ X_{LiBr\ 5}) = \dot{G}_5 h_{sol}(t_5,\ X_{LiBr\ 5}) - \dot{G}_5 h_{sol}(t_6,\ X_{LiBr\ 5}) \quad (21)$$

The procedure of determination and numerical integration of differential heat and mass transfer formulae (Eqs. (14)–(20)) have been demonstrated in detail in the next section describing simulation procedures for the horizontal tube banks falling-film absorber. The approaches used for other falling-film exchangers were analogous bearing in mind their individual conditions of heat/mass transfer.

The system of 21 non-linear equations was solved by a modified Newton's method (hybrid Powell's method) available in the form of a FORTRAN code as a part of the numerical library MINPACK [12].

3. Modelling of heat/mass transfer phenomena in the falling-film exchangers – a horizontal tube banks absorber

The horizontal tube banks geometry coupled with the gravitationally falling laminar film of the absorbent effects in the cross-current regime of mutual flow for the working fluids. The geometry arrangement is not the issue for mass transfer since the H_2O vapour filling the absorber container is well-mixed, hence it may be assumed that thermal parameters of the H_2O vapour are uniform inside the gaseous volume of the absorber [6,9].

The presented approach is derived from classic Nusselt solution for the plate-type heat exchanger, based on the heat transfer equation and energy balances along with the following main assumptions [14]:

- both fluids unmixed;
- heat flux perpendicular to the heat exchange area;
- one-dimensional heat transfer modelled by means of one-dimensional conduction and the heat transfer coefficients for convection.

The authors adapted Nusselt's method for the horizontal tube-type absorber analysis, which implies:

- the standard Cartesian coordinate system changed into the cylindrical coordinate system (see Fig. 3), according to the directions of flow for the cooling water (coordinate l) and laminar film of solution (coordinate θ);
- the mass transfer equation (Eq. (23)) attached to the heat transfer equation (Eq. (22)) together with the mass transfer coefficients for modelling of one-dimensional mass transfer;
- convective heat transfer between the H_2O vapour and film neglected due to small values of the convective heat transfer coefficient [4,6,9];
- LiBr–water solution as a Newtonian fluid; gravitational flow of a laminar film described according to Nusselt solution for the film thickness [8]: $\delta = \sqrt[3]{3/4\ \mathrm{Re}_{sol}(\nu^2/g\sin\theta)}$ and conductive heat transfer regime in the laminar film [4,16];
- assumption of symmetry – identical solution flow rates for both outer half-perimeters of each tube as well as the uniform flow distribution of the cooling water inside the tubes (alongside the inner half-perimeters); flows for both fluids for each tube are thus halved vertically (together with the tube) and the model equations are formulated for only one (left or right) side.

According to Nusselt's formulation, the second-order differentials of the heat transfer rate and diffusive mass flow rate are expressed in cylindrical coordinates l and θ as follows:

$$d^2\dot{Q}_{ABS} = \frac{U_l}{2\pi}(t_{sol\ es} - t_{cw})\,dl\,d\theta \quad (22)$$

$$d^2\dot{G}_{dif\ ABS} = \frac{\chi_l}{2\pi}(W_{eq} - W)\,dl\,d\theta \quad (23)$$

The driving force for heat transfer $\Delta t = (t_{sol\ es} - t_{cw})$ is defined as a temperature difference between the external surface of the solution film and cooling water (radial distribution of the cooling water temperature is assumed uniform except the boundary layer [9], modelled by using the heat transfer coefficient [2,3,6], see Figs. 3 and 4). The driving force for mass transfer $\Delta W = (W_{eq} - W)$ is identified as a mass ratio difference between the external surface of the solution film and solution film interior (radial distribution of LiBr concentration is assumed uniform except the mass transfer layer [9], modelled by using the mass transfer coefficient [2,3,13], see Figs. 3 and 4). The external face of the film was regarded as a surface in thermodynamic equilibrium conditions [4,6,9,13,18,19], therefore $W_{eq} = f(p,\ t)$.

It should be also emphasised that the values of heat and mass transfer coefficients were determined separately for each discrete fragment of the heat/mass transfer active area, which makes the local character of the heat and mass transfer analysis even more evident.

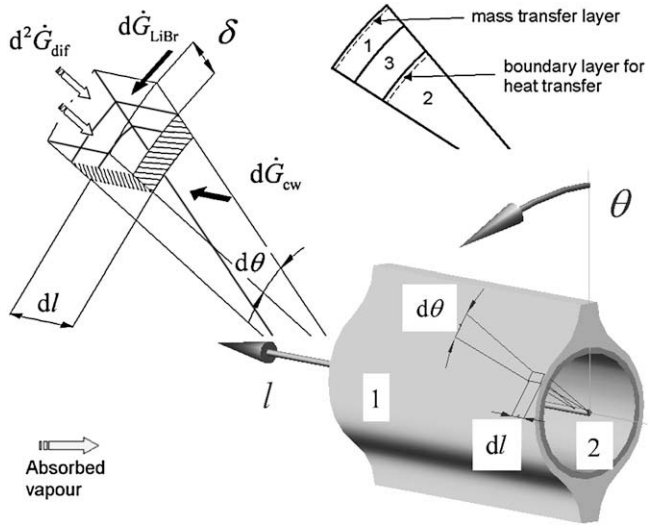

Fig. 3. Schematic representation of an infinitely small fragment of the active heat and mass transfer area for the falling-film horizontal tube banks absorber; 1 – gravitationally falling-film of LiBr–H_2O solution (flow along θ coordinate), 2 – cooling water (flow along l coordinate), 3 – horizontal tube.

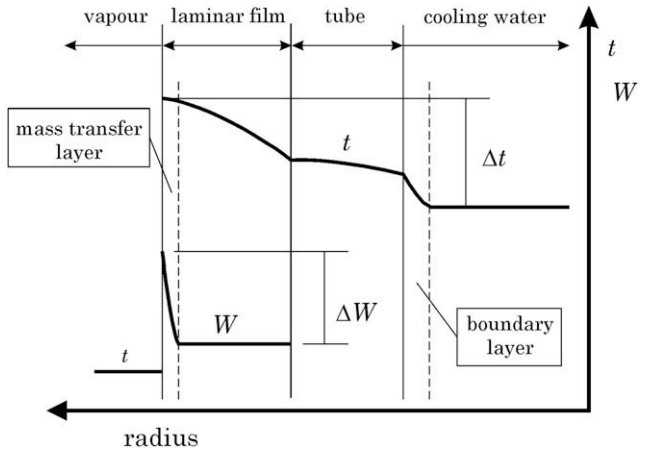

Fig. 4. Schematic representation of the temperature and mass ratio profiles along the tube radius assumed in the absorber model (thickness of particular zones not to scale).

To complete the description of the model, the mass and energy balances for an infinitely small element of heat and mass transfer $\mathrm{d}l\,\mathrm{d}\theta$ may be formulated (see Fig. 3), as follows:

- Solution mass balance,

$$d^2\dot{G}_{\text{dif ABS}} = \mathrm{d}\dot{G}_{\text{LiBr}}\,\mathrm{d}W|_{\text{l=idem}} = \frac{\dot{G}_{\text{LiBr}}}{L}\frac{\partial W}{\partial\theta}\,\mathrm{d}l\,\mathrm{d}\theta \tag{24}$$

- Cooling water energy balance,

$$d^2\dot{Q}_{\text{ABS}} = \mathrm{d}\dot{G}_{\text{cw}}\,\mathrm{d}h_{\text{w}}|_{\theta=\text{idem}} = \frac{\dot{G}_{\text{cw}}c_{\text{cw}}}{\Theta}\frac{\partial t_{\text{cw}}}{\partial l}\,\mathrm{d}l\,\mathrm{d}\theta \tag{25}$$

- Solution energy balance,

$$\begin{aligned} d^2\dot{Q}_{\text{ABS}} &= -\mathrm{d}\dot{G}_{\text{LiBr}}d[(W+1)h_{\text{sol}}]|_{l=\text{idem}} + d^2\dot{G}_{\text{dif ABS}}h''_{\text{v}} \\ &= \frac{\dot{G}_{\text{LiBr}}}{L}\left(C_1\frac{\partial W}{\partial\theta} + C_2\frac{\partial t_{\text{sol}}}{\partial\theta}\right)\mathrm{d}l\,\mathrm{d}\theta \end{aligned} \tag{26}$$

where coefficients C_1, C_2 are defined as follows:

$$C_1 = h''_{\nu} - h_{\text{sol}} - (W+1)\frac{\partial h_{\text{sol}}}{\partial W} \tag{27}$$

$$C_2 = -(W+1)\frac{\partial h_{\text{sol}}}{\partial t_{\text{sol}}} \tag{28}$$

The quantity denoted as $\dot{G}_{\text{LiBr}} = \dot{G}_{\text{sol}}X_{\text{LiBr}}$ expresses the mass flow rate of pure lithium bromide that is equally distributed along half a tube.

The second-order differentials in Eqs. (22)–(26) can be eliminated by the mathematical transformation. As a result, it is possible to develop a system of the partial differential equations (Eqs. (29)–(31)) including four main field unknown variables: $W = 1 - X_{\text{LiBr}}/X_{\text{LiBr}}$, t_{cw}, t_{sol} and $t_{\text{sol es}}$:

$$\frac{\partial W}{\partial\theta} = \frac{\chi_{\text{l}}(W_{\text{eq}} - W)L}{2\pi\dot{G}_{\text{LiBr}}} \tag{29}$$

$$\frac{\partial t_{\text{cw}}}{\partial l} = \frac{U_{\text{l}}(t_{\text{sol es}} - t_{\text{cw}})\Theta}{2\pi\dot{G}_{\text{cw}}c_{\text{cw}}} \tag{30}$$

$$\frac{\partial t_{\text{sol}}}{\partial\theta} = -\frac{1}{C_2}\frac{L}{2\pi\dot{G}_{\text{LiBr}}}\left[C_1\chi_{\text{l}}(W_{\text{eq}} - W) - U_{\text{l}}(t_{\text{sol es}} - t_{\text{cw}})\right] \tag{31}$$

The third unknown field variable t_{sol} constitutes in fact the radial average temperature of a laminar LiBr–water film. The distribution of the solution temperature along the radial coordinate is derived from the assumption of the heat transfer regime in the laminar film considered to be pure conductive heat transfer. This simplification allows the extraction of $t_{\text{sol es}}$ variable from Eqs. (30) and (31) which leads to further reduction of the final number of the unknown field functions in Eqs. (29)–(31) to three: $W = f_1(l,\,\theta)$, $t_{\text{cw}} = f_2(l,\,\theta)$, $t_{\text{sol}} = f_3(l,\,\theta)$.

The calorific functions for liquid LiBr–H_2O mixture can be easily found in technical and scientific literature and databases [5,6,10,19] along with other physical properties, including density, specific heat capacity, thermal conductivity, viscosity, mass diffusion coefficients, surface tension, etc.

Taking into account the assumption of a uniform solution flow alongside both outer tube half-perimeters and uniform flow distribution of the cooling water inside the tubes, along with specified boundary conditions, it is possible to obtain the complete field of the unknown variables for a single tube by numerical integration for only a half of the tube, expecting the solution to be ideally symmetrical for both parts. Due to relatively simple geometry of the absorber active area and proved computational simplicity and effectiveness the Finite Difference Method was applied to solve Eqs. (29)–(31).

In addition, an implementation of further simplifications enables one to find the complete distribution of the unknown fields for the whole heat and mass transfer effective area in the absorber, i.e. the banks of tubes arranged into rows and columns (see Fig. 5). The extra assumptions are as follows [9]:

- ○ solution sprinkling density is uniform along the tube length and identical for each vertical column of tubes,
- ○ the absorption process for each column of tubes is not affected by the neighbouring columns,
- ○ distribution of cooling water flow is uniform and identical for every tube in the bunch.

Thus, the film temperature boundary conditions for each tube in the column (except the first ones below the sprinkler) are determined by the temperature distribution calculated for the upper neighbouring tube. The complete field of the unknown variables may be obtained by multiplication of the solution for the single column.

On the basis of the calculated distributions, the mean values of the outlet LiBr concentration expressed by H_2O to LiBr mass ratio in Eq. (32) and outlet cooling water temperature (Eq. (33)) for a single column may be determined by integration (see Fig. 5):

$$\overline{W} = \frac{1}{L}\int_0^L W_{i=\text{m}}(l,\,\theta=\pi)\,\mathrm{d}l \tag{32}$$

$$\bar{t}_{\text{cw}\,i} = \frac{1}{\pi}\int_0^{\pi} t_{\text{cw}\,i}(l=L,\,\theta)\,\mathrm{d}\theta \quad \text{for} \quad i=1,\,\ldots,\,\text{m} \tag{33}$$

where i stands for the tube row index, $i = 1, \ldots, m$. The mean value of the outlet LiBr concentration is obviously identical for each column and therefore $\overline{W}$ stands for the average outlet value for the whole absorber. However, the average value of the cooling water outlet temperature for the whole absorber is calculated through the energy balance comprising flows from each horizontal row.

Based on the difference between the absorber inlet and outlet values of cooling water temperature and solution LiBr concentration, the overall exchanged heat and mass transfer rates may be calculated. The results of computations, repeated for all the supplied representative operation conditions for the absorber (five levels for six variables: pressure, solution mass flow rate, solution

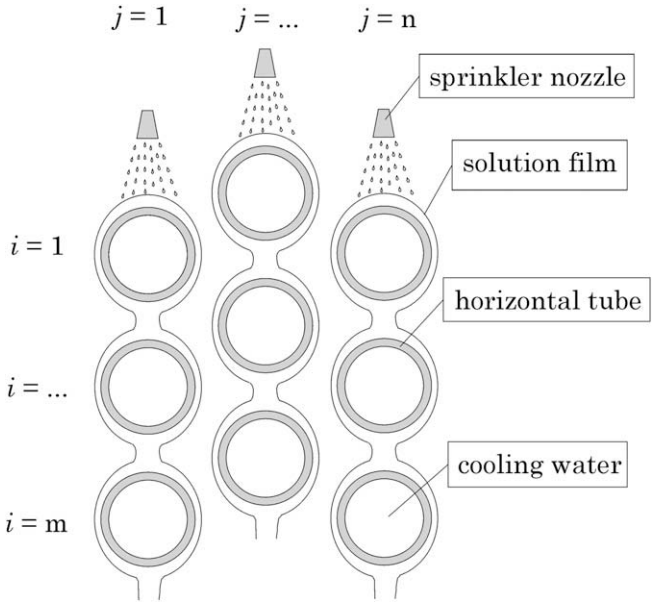

Fig. 5. Schematic representation of geometry arrangement for the falling-film horizontal tube banks absorber (thickness of laminar film not to scale).

temperature, solution LiBr concentration, cooling water mass flow rate and cooling water temperature; $5^6 = 15{,}625$ operating points set up), constitute the database for the approximating procedure (see Fig. 1), which finally leads to an algebraic expression for the total zero-dimensional effect of the absorber operation (Eqs. (14) and (15)).

Due to the crosscurrent flow regime for other heat/mass exchangers, an analogous approach was employed for each component of the model, except the solution heat exchanger which was considered counter-current [21]. Obviously, individual values of heat/mass transfer coefficient were calculated for a particular exchanger, according to the specific character of heat and/or mass exchange conditions.

4. Results of numerical calculations

The basic run of numerical calculations was performed for the input data acquired from technical documentation for a medium-size industrial absorption chiller YORK YIA 6C4 [21], which embraced the geometry, mass flow rates and thermal-parameters. Since the catalogue data was not complete, some part of the input data incorporated into the model was estimated and may be burdened with some discrepancies to the genuine situation (Table 1).

The simulation model can be applied for calculation of distributions of physical parameters of the working fluids as well as to the overall illustration of the chiller energy performance. Figs. 6 and 7 illustrate the example distributions of the LiBr concentration and temperature for a single column of the horizontal half-tubes. To cover the total active area of the absorber the obtained fields were first mirrored and then copied, according to the assumption of symmetry and repeatability. According to Fig. 6, the LiBr mass fraction is constantly decreasing along the flow of the laminar film. However, the influence of the crosscurrent cooling water flow is noticeable: the exit LiBr concentration (last, 11th row of tubes according to the gravitational film flow, equivalent to dimensionless angle of flow $\psi = 11$) is lower for the water inlet side of the absorber. This fact clearly indicates that the diffusive mass flux is non-uniform over the whole active area of the absorber due to the non-uniform distribution of the solution temperature, as illustrated

Table 1
Selected construction parameters of the modelled absorption chiller based on the data for York YIA 6C4 [21].

Element	Construction parameters	Fouling factor, $m^2\,K\,W^{-1}$
Absorber	385* 95/5 Cu/Ni bare* tubes (35 columns × 11 rows), in-line tube bank, tube outer diameter 19.1 mm, tube thickness 0.7 mm, tube length 6.8 m*	0.000088
Desorber	115* 95/5 Cu/Ni bare* tubes (23 columns × 5 rows), in-line tube bank, tube outer diameter 19.1 mm, tube thickness 0.89 mm, tube length 6.8 m*	0.000088
Condenser	187* 95/5 Cu/Ni bare* tubes (17 columns × 11 rows), in-line tube bank, tube outer diameter 19.1 mm, tube thickness 0.7 mm, tube length 6.8 m*	0.000088
Evaporator	260* 95/5 Cu/Ni bare* tubes (26 columns × 10 rows), in-line tube bank, tube outer diameter 19.1 mm, tube thickness 0.7 mm, tube length 6.8 m*	0.000088
Solution heat exchanger	96* 95/5 Cu/Ni bare* tubes (12 columns × 8 rows), in-line tube bank, tube outer diameter 19.1 mm, tube thickness 0.7 mm, tube length 6.8 m*	–
Solution pump	Isentropic efficiency 70%* Electromechanical efficiency 85%*	–

* – estimation.

in Fig. 7. Generally, for the whole active area, the outer surface temperature decreases along the solution flow in the manner similar to the LiBr mass fraction, however small peaks may be visible at the top/bottom of each tube. On the contrary, the inner surface temperature is almost constant along the solution flow over consecutive tubes, while a considerable drop may be observed on the top/bottom of each tube. In addition, the inner surface temperature is evidently higher for the water outlet side of the absorber.

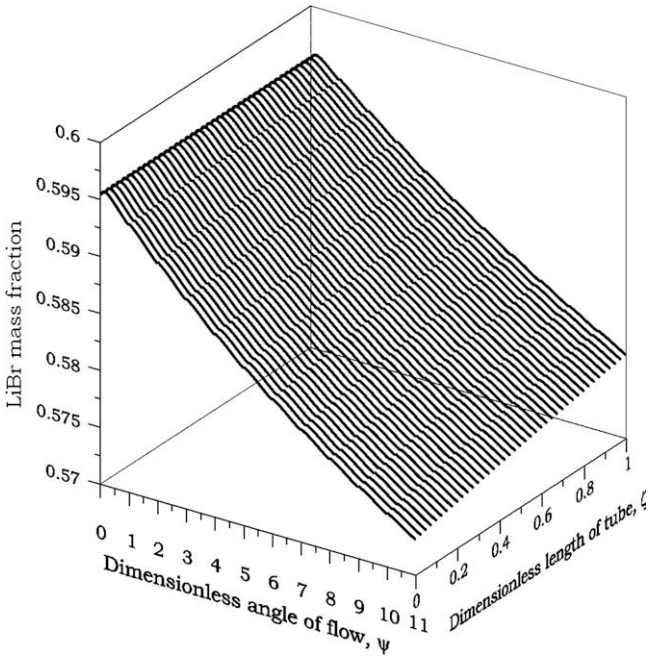

Fig. 6. Simulated two-dimensional distribution of the LiBr concentration in the film interior for a single column of the horizontal half-tubes in the absorber; inlet film temperature: 41.15 °C, inlet film LiBr mass fraction: 59.6%, pressure of absorption: 736 Pa, cooling water inlet temperature: 30.5 °C (for the absorber geometry data see Table 1).

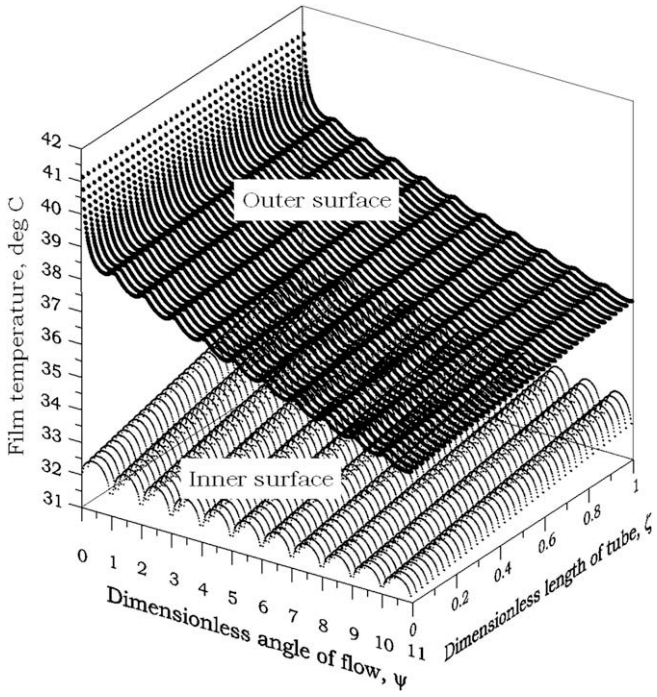

Fig. 7. Simulated two-dimensional distributions of the LiBr–H_2O film temperature for a single column of the horizontal half-tubes in the absorber; inlet film temperature: 41.15 °C, inlet film LiBr mass fraction: 59.6%, pressure of absorption: 736 Pa, cooling water inlet temperature: 30.5 °C (for the absorber geometry data see Table 1).

The simulated profiles prove to be strongly affected by two issues: the crosscurrent flow of working fluids and the laminar film thickness, changeable with the angle of the solution flow. The flow regime inflicts weaker thermal performance on the water outflow side due to higher temperature of cooling water. Greater thickness of the solution film at angles close to 0 and π (approximately two times compared to angle $\pi/2$) reduces heat flux to the cooling water significantly due to increased heat resistance of the laminar film. As a consequence local temperature fluctuations may be recorded. First, the inner surface temperature decreases owing to the heat flux reduction at almost constant values of the cooling water temperature and heat transfer coefficient from the tube to water. Second, the heat flux reduction decreases the diffusive mass flux of vapour and the solution subcooling as a driving force for absorption. Therefore, the outer surface temperature may even rise since the motive difference between the thermodynamic equilibrium temperature and actual temperature is lowered while continuous mass absorption (and consequent enthalpy inflow) takes place at the interface.

However, it must be considered that the shape and magnitude of the recorded local temperature fluctuation is obviously influenced by assumptions of the adapted Nusselt solution, mainly heat and mass fluxes perpendicular to the heat exchange area. Such an approach neglects thermal conduction in other (angular and longitudinal) directions, especially valid for copper tubes of high heat conductivity, which probably amplifies the recorded local phenomena.

An example set of the thermal performance data for a single part-load operation point is presented in Table 2. The system response is consistent with fundamentals of thermodynamics within the range of residuals of the constituting 21 equations, which were arbitrarily set at the level of $1 \cdot 10^{-6}$ [9]. The simulated LiBr mass fraction difference in the thermal pump circuit equal to 5% (the difference between 63.6% for the desorber outlet and 58.6% for the desorber inlet, see Table 2) as well as the coefficient of performance equal to 0.69 are typical values for this range of the hot water inlet temperature, cooling water inlet temperature and circulation ratio [21]. Another interesting effect reported in practice, resulted from the crosscurrent flow regime and superheated conditions of the LiBr–H_2O solution for the desorber, is slight difference in temperature for the outlet vapour (87.5 °C) and outlet strong solution (89.0 °C) [21].

Figs. 8 and 9 present an example of the partial capacity and COP characteristics obtained by approximation of the numerical experiments carried out for a large number of discrete operating points. Both characteristics present typical thermal performance of the LiBr–H_2O absorption chillers at different levels of the hot water and cooling water inlet temperature [9]. In Fig. 8 a significant growth of refrigeration capacity is observed with the increasing value of the hot water inlet temperature and decreasing value of the cooling water inlet temperature. Similarly, the COP increases with the descending value of the cooling water inlet temperature. However, the maximum COP value may be noticed when analysing the influence of the hot water inlet temperature. Moreover, an area of specific temperature conditions at which capacity is reduced to zero can be found in the graph. This fact results from too high cooling water inlet temperature which inflicts too high desorption pressure for a given value of the hot water inlet temperature to desorb the water vapour from the LiBr–H_2O solution. In fact, the minimum level of the desorption temperature is the thermodynamic equilibrium temperature at which the LiBr concentration at pressure of desorption (equal to the pressure of condensation, governed by the cooling water temperature) would reach the LiBr concentration at pressure and temperature of absorption, which would stop the absorption–desorption cycle. The determined idle region characterised by the inlet cooling water temperature values above 34–38 °C along with the inlet hot water temperature values below 75–80 °C agree quite well with the data found in the literature [9].

Since some input data for the model were quite uncertain (partially geometry, circulation ratios for the solution and condensate pump as well as control system settings), it was not reasonable to undertake any validation trial for the complete

Table 2
Simulation results for an example part-load operation point.

Driving parameter (input data)	
Pressure of hot water	8 bar
Pressure of cooling water	5 bar
Pressure of chilling water	5 bar
Inlet temperature of hot water	100 °C
Inlet temperature of cooling water	30.5 °C
Inlet temperature of chilling water	10 °C
Mass flow rate of hot water	47.5 kg s^{-1}
Mass flow rate of cooling water	141.5 kg s^{-1}
Mass flow rate of chilling water	57.2 kg s^{-1}
Circulation ratio	12.8
System response (output data)	
Pressure of absorption	760 Pa
Pressure of desorption	6230 Pa
Refrigerant mass flow rate	0.32 kg s^{-1}
Solution mass flow rate for the absorber inlet/outlet	8.45/8.77 kg s^{-1}
Solution mass flow rate for the desorber inlet/outlet	4.12/3.80 kg s^{-1}
Solution LiBr mass fraction for the absorber inlet/outlet	0.609/0.586
Solution LiBr mass fraction for the desorber inlet/outlet	0.586/0.636
Solution temperature for the absorber inlet/outlet	44.2/33.2 °C
Solution temperature for the desorber inlet/outlet	60.0/89.0 °C
Strong solution temperature for the solution heat exchanger outlet	57.6 °C
Vapour temperature for the condenser inlet	87.5 °C
Outlet temperature of hot water	94.5 °C
Outlet temperature of cooling water	33.7 °C
Outlet temperature of chilling water	6.7 °C
Chilling capacity	760 kW
Coefficient of performance	0.69

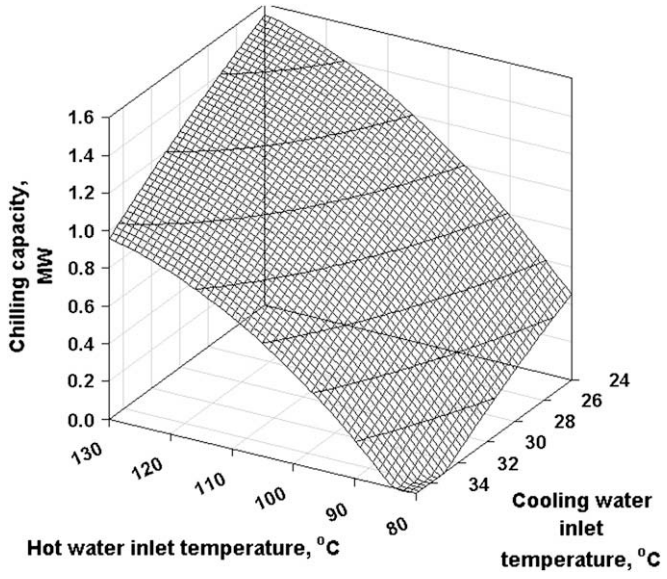

Fig. 8. Approximated partial refrigeration capacity characteristics; chilling water inlet temperature: 12 °C, cooling water mass flow rate: 120 kg/s, hot water mass flow rate: 35 kg/s, chilling water mass flow rate: 80 kg/s (for the chiller geometry data see Table 1).

model. Instead, based on the data found in the broadly cited literature, a verifying investigation for the absorption process modelling only was carried out. Specifically, Seol and Lee in [17] revealed the experimentally measured values of the solution temperature and concentration for the water vapour absorption process over a single horizontal tube (length: 1 m; external diameter: 19.05 mm) for the LiBr–H_2O solution within the following range of process parameters: the solution inlet temperature from 32 to 50 °C, the cooling water inlet temperature from 32 to 50 °C, the pressure of absorption from 530 to 1330 Pa, the solution LiBr mass fraction from 0.6 to 0.62, solution volumetric flow rate from $3.33\cdot10^{-6}$ to $8.33\cdot10^{-6}$ m^3 s^{-1}.

The key issue influencing the absorber model performance is an appropriate selection of the empirical correlation for Sherwood number, indispensable for the determination of the overall mass transfer coefficient introduced in Eq. (23) and further referenced in Eqs. (29) and (31). In addition, when a turbulent flow regime for solution is recognised or unusual conditions are identified (enhanced surface, flow inverters, etc.), it is possible to eliminate the assumption of heat conduction in the laminar solution film and introduce proper (matching to the particular conditions) empirical correlations for the solution Nusselt number. Since individual conditions of heat and mass transfer may lead to different forms of the correlation formulae (even for the same configuration of gravitational flow of solution over a horizontal tube) it is always reasonable to evaluate the data accessible in the literature. An example set of the selected correlations for Sherwood number analysed in this work is listed in Table 3, whereas their correspondence to the results of Seol's and Lee's experiment [17] is presented in Fig. 10.

In most cases the results of simulation are located within the range of the measurement accuracy. Therefore, the observed consistency between the output data from the absorber model and experiment seems to be satisfactory. However, it may be noticed that the feature of the model may be to some extent quantitatively and qualitatively sensitive for the Sherwood number as well as Nusselt number correlations. This remark is also valid for other analysed heat/mass transfer exchangers. Therefore, as a first step of the modelling process, it is always advisable to investigate very scrupulously the conditions of heat and mass transfer for each particular exchanger, including the issues of flow regime (turbulent, transitional, laminar) and active area profile (tube banks geometry and material, roughness, surface enhancements, etc.). This individual selection of the correlations for heat and mass transfer dimensionless numbers coupled with the detailed knowledge of technical data for the modelled device should be an indispensable stage of a comprehensive process of the model preparation, verification and validation. The next step of the research will be experimental investigation of the LiBr–water absorption chiller intended for small capacity but constructed according to the technology broadly used by industrial manufacturers (horizontal tube banks heat/mass exchangers, gravitationally flowing solution/refrigerant film, solution jet pump, common cooling water passage for the absorber and condenser, etc.).

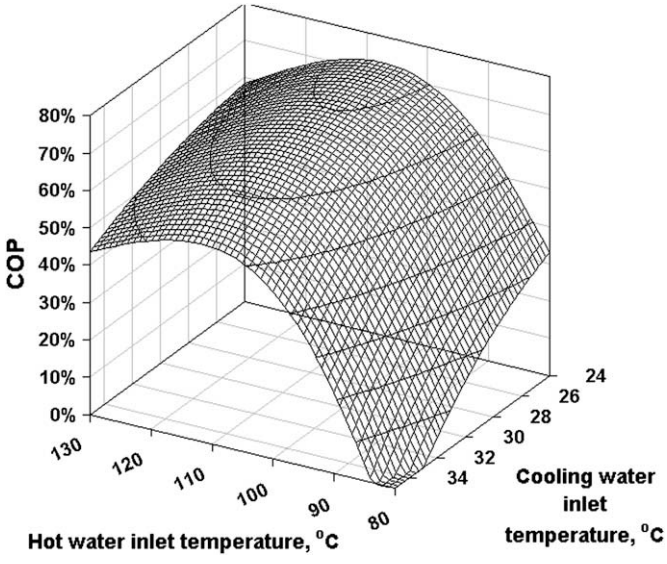

Fig. 9. Approximated partial Coefficient of Performance (COP) characteristics; chilling water inlet temperature: 12 °C, cooling water mass flow rate: 120 kg/s, hot water mass flow rate: 35 kg/s, chilling water mass flow rate: 80 kg/s (for the chiller geometry data see Table 1).

Table 3
Example set of the analysed empirical correlations for Sherwood number for absorption on a horizontal tube.

Correlation for Sherwood number	Characteristic length for Sh number	Source
1 $Sh_{sol} = 0.01144\ Re_{sol}^{0.86}\ Sc_{sol}^{0.5}$	Solution film thickness at $\theta = 90°$	[13]
2 a) $Sh_{sol} = 0.03725\ Re_{sol}^{0.2715}\ Sc_{sol}^{0.5}$ for $100 < Re_{sol} < 700$ b) $Sh_{sol} = 0.002326\ Re_{sol}^{0.6938}\ Sc_{sol}^{0.5}$ for $700 < Re_{sol} < 1300$	Cube root of a ratio of kinematic viscosity squared to gravitational acceleration	[3]
3 $Sh_{sol} = 3.76\ Re_{sol}^{-0.33}$	Cube root of a ratio of kinematic viscosity squared to gravitational acceleration	[18]
4 a) $Sh_{sol} = 1.03\ Re_{sol}^{-0.146}\left(\frac{Sc_{sol}}{1000}\right)^{1.42}$ for $Re_{sol} < \left(\frac{Sc}{5367}\right)^{-3.61}$ b) $Sh_{sol} = 0.094\ Re_{sol}^{0.29}\left(\frac{Sc_{sol}}{1000}\right)^{2.6}$ for $Re_{sol} > \left(\frac{Sc}{5367}\right)^{-3.61}$	Cube root of a ratio of kinematic viscosity squared to gravitational acceleration	[2]

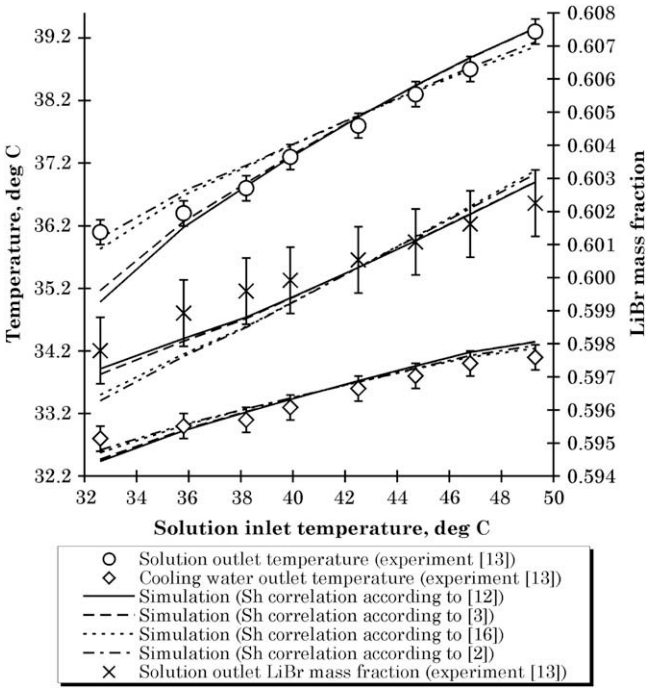

Fig. 10. Variation of solution outlet temperature and LiBr mass fraction with solution inlet temperature – comparison for the experimental apparatus of Seol and Lee [17] and numerical simulations performed by the authors of the present article (vertical bars indicate measurement accuracy); pressure of absorption: 800 Pa; cooling water inlet temperature: 32 °C; solution inlet LiBr mass fraction: 0.6.

5. Conclusions

A mathematical model of a single-stage, lithium bromide-water absorption chiller was developed taking into consideration: (i) crosscurrent flow of fluids for heat and mass exchangers; (ii) two-dimensional distributions of temperature and concentration fields; (iii) local values of heat and mass transfer coefficients; (iv) thermal-parameters-dependent physical properties of working fluids; and (v) exploitation limitations due to the danger of LiBr–water hydrates and ice crystallisation.

The main practical advantage of the model is the possibility of assessing the influence of both the geometry parameters (mainly diameters, lengths and pitches of tubes) and operation parameters (chiefly flow rates and temperature of water streams) on thermal performance (temperature and concentration values in key points of the cycle, refrigeration capacity, coefficient of performance, etc.).

On the basis of the input data for a typical industrial unit, a series of numerical experiments for various configurations of the operation parameters were performed in order to determine the multidimensional energy characteristics of the chiller, which seems to be particularly important for the pre-investment feasibility analyses that may require the simulation scenarios for differentiated exploitation conditions, very often at part-load refrigeration capacity. However, to obtain a set of characteristics that satisfactorily fit the genuine performance of a typical industrial unit it is crucial to possess complete technical information including detailed schemes of the unit, composition of the working solution as well as the unit control system settings.

The results derived from the implementation of the water vapour absorption process model for a horizontal tube absorber are consistent with the experimental measurements found in the literature. Nevertheless, due to certain model sensitivity to the correlations for heat and mass transfer analogy numbers, it is always indispensable to analyse and determine genuine conditions of heat and mass transfer processes to select the most appropriate approach.

References

[1] M.B. Arun, M.P. Maiya, S.S. Murthy, Equilibrium low pressure generator temperatures for double-effect series flow absorption refrigeration system, Applied Thermal Engineering 20 (2000) 227–242.
[2] F. Babadi, B. Farhanieh, Characteristics of heat and mass transfer in vapor absorption of falling film flow on a horizontal tube, International Communications in Heat and Mass Transfer 32 (2005) 1253–1265.
[3] Y. Chen, Ch Sun, Experimental study on the heat and mass transfer of a combined absorber-evaporator exchanger, International Journal of Heat and Mass Transfer 40 (4) (1997) 961–971.
[4] A. Conlisk, Analytical solutions for the heat and mass transfer in a falling film absorber, Chemical Engineering Science 50 (4) (1995) 651–660.
[5] F-Chart Software, Engineering Equation Solver See also:, Madison, USA, 2003 http://www.fchart.com/ees/ees.shtml Academic Version 6.867-3D.
[6] G.A. Florides, S.A. Kalogirou, S.A. Tassou, L.C. Wrobel, Design and construction of a LiBr–water absorption machine, Energy Conversion & Management 44 (2003) 2483–2508.
[7] H.M. Hellmann, G. Grossman, Simulation and analysis of an open-cycle dehumidifier–evaporator–regenerator (DER) absorption chiller for low grade heat utilisation, International Journal of Refrigeration 18 (3) (1995) 177–189.
[8] S. Jeong, S. Garimella, Falling-film and droplet mode heat and mass transfer in a horizontal tube LiBr/water absorber, International Journal of Heat and Mass Transfer 45 (2002) 1445–1458.
[9] K.A. Joudi, A.H. Lafta, Simulation of a simple absorption refrigeration system, Energy Conversion & Management 42 (2001) 1575–1605.
[10] D.S. Kim, C.A.I. Ferreira, Solar absorption cooling, 1st progress report Report K-332, Delft University of Technology, NL, 2003, pp. 57–63.
[11] F. Mandani, H. Ettouney, H. El-Dessouky, LiBr-H_2O absorption heat pump for single-effect evaporation desalination process, Desalination 128 (2000) 161–176.
[12] J. Moré, B. Garbow, K. Hillstrom, User guide for MINPACK-1, Technical Report ANL-80–74, Argonne National Laboratory, Argonne (USA) See also: http://www.netlib.org/minpack/ (1974).
[13] T. Nosoko, A. Miyara, T. Nagata, Characteristics of falling film flow on completely wetted horizontal tubes and the associated gas absorption, International Journal of Heat and Mass Transfer 45 (2002) 2729–2738.
[14] W. Nusselt, Eine neue Formel für den Wärmedurchgang im Kreuzstrom, Techn Mech Thermodyn Bd 1 (1930) 417.
[16] V. Patnaik, H. Perez-Blanco, Roll waves in falling films: an approximate treatment of the velocity field, International Journal of Heat and Fluid Flow 17 (1996) 63–70.
[17] S. Seol, S. Lee, Experimental study of film flow and heat/mass transfer in LiBr–H_2O solution flowing over a cooled horizontal tube, International Communications in Heat and Mass Transfer 32 (2005) 445–453.
[18] T. Sherwood, R. Pigford, Absorption and Extraction, McGraw-Hill, New York, 1952, pp. 266, 267, 271.
[19] Solar Energy Laboratory, TRNLIB – Libraries of User-Written TRNSYS Components See also:, The University of Wisconsin-Madison (USA), 2003 http://sel.me.wisc.edu/trnsys/default.htm.
[20] G.P. Xu, Y.Q. Dai, Theoretical analysis and optimization of a double-effect parallel-flow-type absorption chiller, Applied Thermal Engineering 17 (2) (1997) 157–170.
[21] York International Corporation. MILLENNIUM YIA Single-Effect Absorption Chillers Tech Guide, York (USA) 1997. See also: http://www.johnsoncontrols.com/publish/us/en/products/building_efficiency/products/Industrial___Commercial_HVAC_Equipment/chiller_products/absorption__single-stage.html,http://www.york.com/products/esg/servicelit/ywpubs/155.16-OM1.pdf